Peertechz

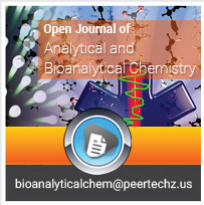

CHEMISTRY GROUP

OPEN JOURNAL OF Analytical and Bioanalytical Chemistry OPEN ACCESS JOURNAL

ISSN: 2689-7628 DOI: https://dx.doi.org/10.17352/ojabc

Research Article

Porous carbon derived from *Zea mays* cobs as excellent electrodes for supercapacitor applications

Moses Kigozi[1,2]*, Richard K Koech[1], Kingsley Orisekeh[1], Ravi Kali[3], Omar LM Kamoga[2], Balaji Padya[3], Abdulhakeem Bello[1], Gabriel N Kasozi[4], Pawan Kumar Jain[3], John Baptist Kirabira[5], Azikiwe Peter Onwualu[1] and Nelson Y Dzade[6]*

[1]Department of Materials Science and Engineering, African University of Science and Technology P.O. BOX 681 Garki, Abuja, Nigeria

[2]Department of Chemistry, Faculty of Science and Education, Busitema University P.O BOX 236 Tororo, Uganda

[3]Centre for Carbon Materials, International Advanced Research Centre for Powder Metallurgy & New Materials (ARCI), Balapur P. O 500 005 Hyderabad India

[4]Department of Chemistry, College of Natural Science, Makerere University, P.O BOX 7062, Kampala, Uganda

[5]Department of Mechanical Engineering, Makerere University, P.O BOX 7062, Kampala, Uganda

[6]School of Chemistry, Cardiff University, Main Building, Park Place, CF10 3AT, Cardiff, United Kingdom

Received: 27 January, 2023
Accepted: 08 February, 2023
Published: 09 February, 2023

***Corresponding author:** Moses Kigozi, Lecturer, Department of Chemistry, Faculty of Science and Education, Busitema University P.O BOX 236 Tororo, Uganda, Tel: +256772609744;
E-mail: mkigozi@aust.edu.ng

ORCiD: https://orcid.org/0000-0002-6463-9052

Nelson Y Dzade, School of Chemistry, Cardiff University, Main Building, Park Place, CF10 3AT, Cardiff, United Kingdom, E-mail: DzadeNY@cardiff.ac.uk

Keywords: Excellent stability; High capacitance; KOH activation; Porous carbon; Supercapacitor application; *Zea mays* cobs

Abstract

Improving the efficiency of the electrode materials is critical for achieving high performance in supercapacitors. Porous carbon with appropriate designs is dependable for better electrochemical capacitors. In this work, we improved *Zea mays* (maize) cobs as a potentially plentiful precursor for generating porous carbon supercapacitor applications. The physical and chemical properties of the synthesized materials were determined using several approaches, including structure, morphology, chemical composition, and electrochemical performance. The chemical analyses revealed an oxygen-based surface structure, while structural analysis revealed a BET-specific surface area of 1443.94 m^3/g and a pore volume of 0.7915 cm^3/g. Symmetric devices based on the materials generated had a specific capacitance of 358.7F/g, an energy density of 12.45 Wh/kg and a power density of 250 W/kg at 0.5A/g. The as-prepared electrodes demonstrated exceptional stability, with a capacitance retention of 99% at the maximum potential for a total of 130 hours of testing.

Citation: Kigozi M, Koech RK, Orisekeh K, Kali R, LM Kamoga O, et al. (2023) Porous carbon derived from *Zea mays* cobs as excellent electrodes for supercapacitor applications. Open J Anal Bioanal Chem 7(1): 001-010. DOI: https://dx.doi.org/10.17352/ojabc.000028

Introduction

Technology evaluation globally has shown an enormous demand for energy consumption. This is due to the increasing population, and the number of gadgets developed to simplify life. Generation Alpha's interaction with artificial intelligence and automated voice is becoming integral to standard systems, impacting health, life, and future generations. All these aspects require power to be renewable and sustainable. Renewable energy harvested from sources like solar/ hydro, wind, and geothermal, among others, is not produced continuously because they are time and weather-dependent. To improve these technologies and become sustainable, energy storage accumulators such as supercapacitors and batteries are required [1,2]. Supercapacitors (SCs) have attracted tremendous attention in today's energy storage research due to their excellent performance of high power density, high cycling stability, and quick charge/discharge process [1-4].

Supercapacitors are classified according to their energy storage mechanism, which includes: (i) electrical, chemical double-layer capacitors (EDLC), which store their energy by accumulating charges in a Helmholtz double-layer interaction between electrolyte and electrode, (ii) pseudocapacitors, which store their energy through a reversible faradic redox reaction between electrolyte and electrodes [1-3,5] and (iii) hybrid supercapacitors EDLC electrode materials (Activated Carbon (AC)) offer distinct qualities such as high volume/low density and a large specific surface area, which promotes optimum porosity, wettability, high electrolytic ion adsorption, and superior electrical conductivity [3]. Activated Carbon (AC) is a popular electrode material for supercapacitors produced by activating biomass. This is because biomass is both economically viable and abundant in nature [3,4,6]. Recently, AC materials have been obtained chiefly from renewable and sustainable resources such as agricultural crop wastes, biomass, and residential waste, all of which are environmentally beneficial and renewable [6,7].

There are generally two main activation processes, physical and chemical, used to synthesize AC from biomass. Chemical activation is commonly used because of its low activation time, low temperatures, uniform pore size distribution, high yield, and controllable specific surface area compared to the physical process [5]. The chemical activation commonly employs activation agents, including potassium hydroxide (KOH), sulphuric acid (H_2SO_4), sodium hydroxide (NaOH), phosphorous acid (H_3PO_4), zinc chloride ($ZnCl_2$), among others which are extensively applied at different temperatures and different atmospheres [6,8]. Several articles on EDLC supercapacitors have reported different AC from biomass and other materials, including African maize corn cob with SSA of 254 m^2/g and a specific capacitance of 456 F/g at a specific current of 0.25 A/g [5]. The waste tea with an SSA of 294.6 m^2/g exhibited a specific capacitance of 199 F/g at the specific current of 0.5A/g. The SSA range of 1308 m^2/g gave a specific capacitance of 140 F/g at a current density of 0.1A/g from Waste tea [7]. Rosewood and corn cob [9], banana peels [10], corn husk with SSA of 1370 m^2/g, and a specific capacitance of 127 F/g at 1 A/g [6] were reported. Pinecones with SSA of 1169.31 m^2/g show a specific capacitance of 43 F/g at 0.5 A/g [3], coconut shells exhibited SSA of 11614 m2/g resulting in a high capacitance of 426 F/g at 0.5 A/g with electronic conductivity of 11.43 S/cm [11]. Tongcao biomass was reported to have an SSA of 1425.2 m^2/g with a gravimetric capacitance of 244.51 F/g at a scan rate of 20 mV/s [4]. Lastly, nitrogen-doped porous carbon (NPC)/mesophase pitch exhibited an SSA of 503.8 m^2/g with a specific capacitance of 232.2 F/g at 2 A/g [12].

Generally, in EDLC, the charge is stored at the interface of the electrolyte/electrode system. This is primarily controlled by a high specific surface area (SSA) with the appropriate distribution of the pore volume (micropores, mesopores, and macropores) of the materials for the electrode to improve the electrochemical performance. When carrying out the activation of biomass for carbon-derived material for supercapacitors, the process needs to be optimized for improved high SSA and adequate distribution of the pore volume, which can enhance the electrochemical storage performance [5]. It has been shown that a high SSA with an adequate distribution of mesopores and micropores is a vital parameter necessary to obtain a better performance of porous EDLCs carbon electrodes. Still, a definite relationship between the capacitance and SSA has not been clearly shown [13,14]. Porous carbon is favorable because the pore structure governs the material's measured capacitance, energy storage, and power delivery capability. BET contribution results exhibited micropores' total surface and larger pores' surface (mesopores and macropores) [13]. It is worth stating that the macropores (> 50 nm) make virtually no contribution to the total capacitance. Still, it acts as the ion buffering reservoir [15]. In comparison, micropores (< 2 nm in size) serve as the ion traps for energy storage, and mesopores (2 < 50 nm) act as the ion transport pathways for power delivery [15,16]. As mentioned earlier, different activation agents are employed to achieve the required porosity and morphology, but the optimization of carbonization and activation temperature is also necessary. This research work aimed to optimize the temperature for activating *Zea mays* cob to improve porosity, morphology, and performance. The activating agent in this study is KOH, the most frequently used for the different biomass activation processes. KOH gives better porosity and significant SSA because of its comprehensive cation, the carbon lattice expansion by K^+ ion intercalation, synergism, and chemical activation [3,17]. The KOH activation provided excellent electrode materials contributing to pseudocapacitance with heteroatoms bonded on the material's surface [18]. Previously, we reported an acid treatment of maize cobs that led to an SSA of 357 m^2/g with good electrochemical performance [5]. In this current work, the *maize cobs*-derived porous activated carbon materials were carbonization at 400 °C for 90 min and KOH activation at different temperatures (600, 700, and 800 °C) using a ratio of 1:4 of the sample with KOH. The produced carbon materials were used to fabricate symmetric devices and tested in two and three-electrode configurations to evaluate the electrochemical performance [19].

Citation: Kigozi M, Koech RK, Orisekeh K, Kali R, LM Kamoga O, et al. (2023) Porous carbon derived from *Zea mays* cobs as excellent electrodes for supercapacitor applications. Open J Anal Bioanal Chem 7(1): 001-010. DOI: https://dx.doi.org/10.17352/ojabc.000028

Experiments

Materials

The *Zea mays* (maize) cobs were obtained from the nearby farms of the African University of Science and Technology (AUST) Abuja. The potassium hydroxide (90% SDFCL), carbon black, PVDF, and NMP (99% Sigma-Aldrich) were used.

Preparation of activated carbon

The Activated carbons nanostructure was prepared as follows; the *Zea Mays* cobs were collected from farmers near the African University of Science and Technology (AUST) Abuja, Nigeria. The cobs were cleaned and sized to approximately ~3 cm^3. The sample was dried in an oven at 110 °C for 48 h, then ground and sieved to fraction using a 1.0 mm sieve. The cobs sample powder was synthesized using two steps at elevated temperatures. First, raw material from the *Zea mays* was carbonized at 400 °C for 90 min with a 3 °C/min ramp under the nitrogen atmosphere. After that, the sample was divided into three (3) portions. These portions were mixed with KOH as the activating agent in a mass ratio of 1:4 and activated using three (3) different temperatures on different days in a furnace under a nitrogen atmosphere with a flow rate of 300 mL/min with a ramped temperature of 3 °C/min and a holding time of 2 h. The first (1^{st}) portion was activated at 600 °C and the sample was named ANN6. The second (2^{nd}) and the third (3^{rd}) portions were heated at 700 °C and 800 °C, then named ANN7 and ANN8, respectively.

Methods

Material characterization

The morphological and elemental composition of the samples was examined by a Field Emission Scanning Electron Microscope ((FESEM) Gemini-SEM 500M/s Carl ZEISS-EDAX Z2 Analyser AMETEK) Bangalore, India. X-Ray Diffraction (XRD) patterns were obtained by Rigaku Smart lab Autosampler XRD scanned from 8 to 100 deg (RIGAKU Corp., Tokyo, Japan) equipped with a Cu kα radiation (wavelength λ = 1.54 Å) and the JCPDS-ICDD database. The samples' Thermogravimetric Analysis (TGA) was executed using a TGA-DSC analyzer (Jupiter STA449 F3 NTZSCH GmbH) Selb, Germany. The samples were heated in pure air at a flow rate of 10 cm^3/min from room temperature to 1000 °C at a ramped temperature of 10 °C/min with a run time of 100 min using a calcinated silica pan as reference material [20-22]. The surface chemistry and functional groups of AC samples were examined by Fourier Transformation InfraRed (FTIR) spectroscopy (Bruker Optik GmbH Vertex 70, Ettlingen, Germany) scanned from 600 to 4000 cm^{-1}. The X-ray Photoelectron Spectroscopy (XPS) method with spectra in the K-alpha Photoelectron spectrometer using omicron Nano Technology London, UK. [23,24]. The activated samples' Nitrogen adsorption and desorption isotherms were obtained using a 77K automated adsorption instrument (11-2370. Gemini Miceomeritics, Atlanta, GA, USA). The AC samples were degassed at 300 °C in a vacuum for 10 hr [5].

Electrochemical characterization

The two and three-electrode systems configuration measurements were employed using BIO-LOGIC (BCS-805) workstation operating on the BT-Lab software. The working electrodes were prepared by mixing the active materials 80%, carbon black 10%, and 10% binder (poly Vinylidene). A few drops of 1-methyl-2-pyrrolidine (NMP) were added to form a uniform paste coated on a graphite foil as the electrode's current collector. The coated electrodes were dried in an electric oven at 70 °C for 15 h. The electrochemical measurements, including Galvanostatic Charge-Discharge (GCD), cyclic voltammetry (CV), Electrochemical Impedance Spectroscopy (EIS), stability, and self-discharge, were examined using 6 M KOH aqueous electrolyte. In the three-electrode configuration system, the as-prepared materials were used as the working electrode, Ag/AgCl as a reference electrode and Pt as the counter electrode. The CV and GCD were measured using a potential range from 0 V to 1.0 V. The two-electrode measurement was carried out with two working electrodes with similar mass loads separated by cellulose filter paper assembled in a Swagelok symmetrical setup with a 6 M KOH aqueous solution. The CV and GCD properties were investigated between 0 V to 1.0 V potential, and the EIS test was performed in the frequency range of 10 kHz to 10 MHz at 10 mV. The stability of the device was carried out with the floating technique (voltage holding) as described in [5,24]. The self-discharge was performed by charging the device to a maximum voltage, held for 5 min, and then left to self-discharge to determine the percentage voltage loss with time as described by [25-27].

The Specific capacitance (c_{sp} F/g) with three-electrode was calculated using GCD equation (1) [2,3,6,12].

$$C_{sp} = \frac{I\Delta t}{m\Delta V} \quad (1)$$

Where; I is the discharge current (A), Δt is the discharge time (s), ΔV is the applied potential window (V) and m is the coated mass of the active materials (g). The specific capacitance of a single electrode in the two-electrode symmetric setup was calculated using equation (2) [2,28].

$$C = 4\frac{I\Delta t}{M\Delta V} \quad (2)$$

Where; C is the capacitance (F/g), I/M is the specific current (A/g), Δt is the discharge time (s) and ΔV is the potential window (V). The energy density (E, Wh/kg) and power density (P, W/kg) of the symmetric device supercapacitor was calculated using the following equations.

$$E = \frac{C(\Delta V)^2}{28.8} \quad (3)$$

$$P = 3600\frac{E}{\Delta t} \quad (4)$$

Results and discussions

Morphology and structural characterization

The morphology of the three activated carbon materials was

Citation: Kigozi M, Koech RK, Orisekeh K, Kali R, LM Kamoga O, et al. (2023) Porous carbon derived from *Zea mays* cobs as excellent electrodes for supercapacitor applications. Open J Anal Bioanal Chem 7(1): 001-010. DOI: https://dx.doi.org/10.17352/ojabc.000028

analyzed by FESEM/EDS, as stated earlier, and the results are shown in Figure 1. The AC samples exhibited irregular sheets with apparent porosities. This implies that the morphology could be from the volatile organics and swell expansion, as reported by Xie, et al. [9] and Wang, et al. [8]. The three-carbon samples had rough surfaces with significant porosity, which created an ideal interface for electrolytic I diffusion and intercalation during the charge-discharge process of the EDLC electrodes. The visible surface porous structure of the samples changed as the temperature changed. ANN6 (Figure 1a) had enormous irregular pores akin to a honeycomb structure comparable to ANN7 (Figure 1b). However, as compared to the ANN6 and ANN7, the ANN8 (Figure 1c) has a more tightly packed structure, which we refer to as improved in-depth porosity. The EDS (Energy dispersive spectroscopy) and the elemental mapping of all three (3) samples confirm the presence of carbon materials with 75% – 99% wt in the activation with KOH. This creates high porosity with the high surface area due to redox reactions and the evolution of volatile organics as gases hence increasing the porosity [29]. The EDS of ANN6 shows that it is 99.48% carbon with trace amounts of silica and sulfur. The ANN7 had 89.47% carbon, as well as silica and calcium. Table 1 and Figure 1 demonstrate that the ANN8 sample contained 75.22% carbon. The increased activation temperature leads to the production of silica groups, resulting in a more excellent silica value in ANN8.

The XRD pattern of the activated carbon was carried out to confirm the phase composition, as shown in Figure 2a. The spectra exhibited familiar firm, broad peaks at 2θ = 23.3° and 43.1° corresponding to (002) and (100) lattice planes for all the samples, respectively [11,30-32]. The peak formation at 2θ = 23.2° with a plane of (002) indicates a graphitic structure and amorphous morphological phase in the derived activated carbon materials [33]. The degree of graphitization is closely related to the conductivity of carbon materials [34]. The JCPDS card no. 41-1487 shows the profile of ANN6 and ANN7 at 2θ = 23 and 40 – 43° with a d-spacing of 4.435 – 4.456 Å and 2.214 – 2.228 Å, respectively. The shift in the 2θ value of ANN8 towards large angles at high-temperature sample leads to the changed d-spacing at 2θ = 26.4° and 43.09° to 3.380 Å and 2.108 Å respectively. This is also visible in their morphology, where ANN8 differs from the other two. In all the 3 samples, the d -spacing at 2θ = 23° is more significant than 3.35 Å (for graphite), indicating the formation of hard carbon [5]. The decrease in d-spacing causes a decrease in non-crystallinity, as shown in Figure 1, between ANN6, ANN7 and ANN8 morphology variation [6].

Figure 2b depicts the FTIR spectra of derived activated carbon. For the skeleton of the materials, the fingerprint area (1500 - 600) revealed three strong primary peaks of C-OH, C-O-C, C-H, C-N, and C-O. In addition, the diagnostic area (4000 - 1500 cm^{-1}) showed the major vibration at 1737 cm^{-1} as the strongest peak for the three samples. This is due to the frequency vibration of the C=O stretching in the structure of aromatic lactone, carboxyl, or quinone groups stretching, which is stronger in activated carbon. sp^3(C-H), sp^2(C-H) stretching vibration (2990 to 3050 cm^{-1}), and O-H/sp stretching vibration

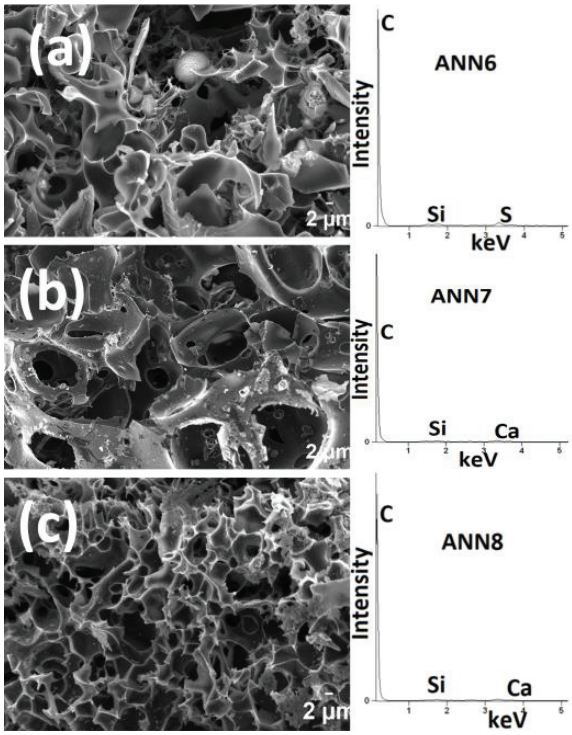

Figure 1: FESEM/EDX morphology and elemental compositions for (a) ANN6, (b) ANN7, and (c) ANN8 carbon samples.

Table 1: EDS elemental composition for ANN6, ANN7, and ANN8 AC samples.

Sample	C	Si	S	Ca
ANN6	99.48	0.48	0.04	-
ANN7	89.47	7.91	-	2.62
ANN8	75.22	18.43	-	6.35

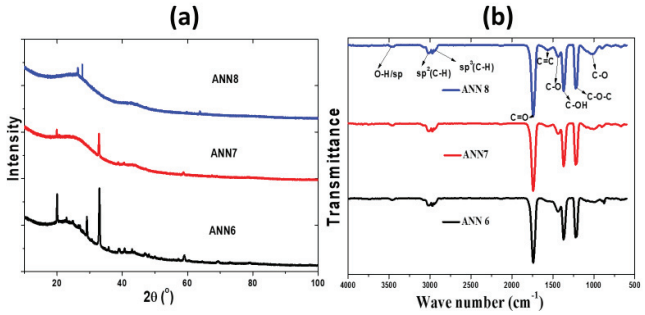

Figure 2: (a) XRD spectra, (b) FTIR spectra for ANN6, ANN7 and ANN8 activated carbon samples.

are also found (3450 cm^{-1}). C-H stretch and out-of-plane bending vibration are responsible for the vibration stretching between 2990 and 3050 cm^{-1}. The fingerprint region showed bending vibrations of C-H or C-N, indicating a dehydrogenation reaction. This is accelerated as the activation temperature rises. The information and frequency vibrations of the functional groups are compatible with the literature [2,12,35].

The composition and functional groups of the samples were further examined by the XPS technique, as shown in Figure 3 and Figure S1 (supplementary information), with their binding energy and assignment of C1s, O1s, and Si2p. The samples

Citation: Kigozi M, Koech RK, Orisekeh K, Kali R, LM Kamoga O, et al. (2023) Porous carbon derived from *Zea mays* cobs as excellent electrodes for supercapacitor applications. Open J Anal Bioanal Chem 7(1): 001-010. DOI: https://dx.doi.org/10.17352/ojabc.000028

exhibited no significant difference in their positions and shapes for different temperature treatments. The deconvolution of the C1s for sample ANN8 in Figure 3, ANN7 and ANN6 spectra Figure 1S (Supplementary information) was observed in five-carbon states as follows; C-C and sp^2 at 284 eV, C-O, C-N at 285.5 eV, C-C at 287.8 eV, O-C=O, C=O at 289 eV. The Si2p exhibited one peak at 102 eV, indicating Si-O, and the O1s showed two oxygen states of C=O at 532 eV and C-O at 534 eV. The spectra states are consistent with the other literature as reported [3,10,36,37]. The designated functional groups of O=C, C-O-H, C-O-C, and others are frequent surface structures of phenolic, ester, quinine, lactonic, and carboxyl groups. The atomic percentages from XPS analyses are shown in Table 2. This showed a significant decrease in carbon and oxygen percentages due to a rise in temperature, which generated an increase in silica percentage at a higher activation temperature [8,38].

The thermogravimetric analysis (TGA/DSC) was carried out to confirm the degradation and purity of the ANN6, ANN7, and ANN8 samples materials. The TGA/DSC data was collected by heating the three samples to 1000 °C under a pure airflow, as shown in Figure 4a, and the TGA data in Table 3. The TGA data collected on the raw material *Zea mays* cobs shown in figure 4a exhibited two distinct decomposition stages; the 1st stage is at a range of 210 °C to 260 °C and the 2nd stage is between 350 to 370 °C. The heat flow through the raw material exhibited exothermal and endothermal flow. The first endothermic phase at 100 °C was due to moisture in the sample. The second endothermic exhibited water loss of crystallization at 360 °C. The heat flow was uniform throughout up to 1000 °C, with the highest exothermal phase at 352 °C with 0.70 mW/mg. The material decomposition was up to 85% mass loss at 1000 °C. ANN6 sample material (Figure 4b) exhibited three decomposition stages; the 1st and 2nd between 45 to 114 °C, the third stage at 286 to 298 °C, and the mass loss as shown in Table 3. The heat flow through ANN6 exhibited endothermic and exothermic flow (Figure 4b). The ANN7 and ANN8 sample materials exhibited two distinct similar decomposition stages. These are consistent with that of ANN6 for the first and second stages. Stage one and stage two decomposition may be due to organic volatile materials and moisture trapped after activation processes. The heat flow through the three materials exhibited the same trend: endothermic at 106 °C and peak exothermic at around 351 °C and 0.91 mW/mg.

The BET approach was used to assess the porosity and specific surface area (SSA) of *Zea mays*-derived activated carbon, as shown in Figure 5. The N_2 adsorption-desorption isotherm was used to calculate the pore volume and specific surface area for the three samples, as shown in Table 4. The samples' isotherms exhibit type I isotherms with micropores, and the hysteresis loop is mainly caused by the mesoporous structure [9]. The hysteresis loop at a relative pressure from 0.4 to 0.9 P/Po in the adsorption-desorption isotherms is mainly because of the presence of mesopores with the formation of interparticle condensation of N_2 at > 0.9P/Po. The calculated SSA for ANN8 exhibited the highest value of 1443.94 m^2/g with a total pore volume of 0.7915 cm^3/g. The samples ANN7 and ANN6 exhibited the SSA of 972.65 and 461.36 m^2/g with a total pore volume of 0.5310 and 0.2464 cm^3/g, respectively, as shown in Table 4. Figure 5b depicts the three samples' pore size distribution, with an average mean pore diameter of 6.39, 7.71, and 7.91 nm for ANN6, ANN7, and ANN8 [13]. The increased surface area and averagely smaller pores make electrode materials suitable for energy storage systems because their shape can induce quick charge transfer, which also contributes to the establishment of EDLC surface interfaces for electrode surfaces and electrolyte ions [3,4,12].

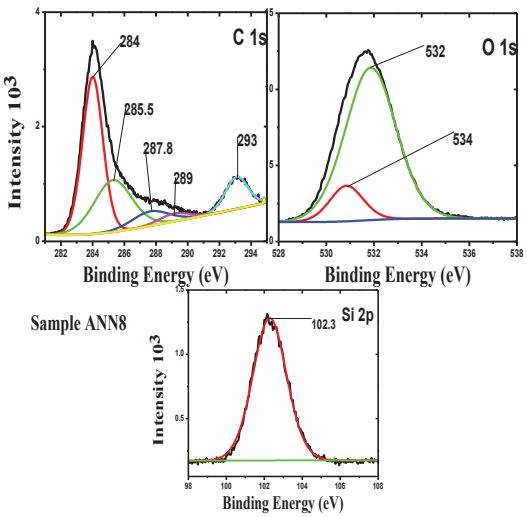

Figure 3: XPS deconvoluted spectra for ANN8 activated carbon sample.

Table 2: Atomic percentages as obtained from XPS analysis.

Sample	Atomic concentration (%)		
	C 1s	O 1s	Si 2p
ANN8	51.86	37.68	10.46
ANN7	75.66	24.08	5.26
ANN6	83.46	14.48	2.05

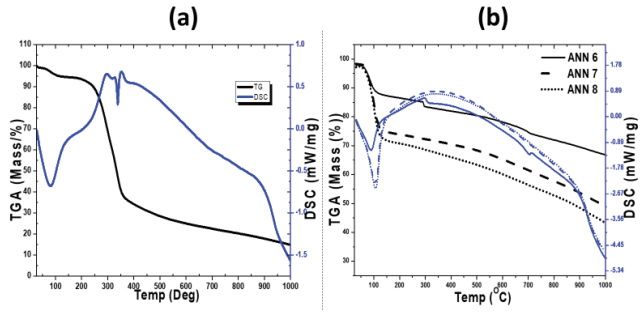

Figure 4: TGA/DSC profile (a) Zea mays cobs and (b) activated carbon ANN6, ANN7 and ANN8 sample materials.

Table 3: TGA/DSC material decomposition of the raw material and activated carbon samples.

Decomposition stages	Mass fraction (%) lost at different stages			
	Raw material	ANN6	ANN7	ANN8
I	10.4	2.1	2.5	2.5
II	63	10.9	23.7	26.1
III		16.4	-	-
At 1000 °C	15.3	67.1	49.3	43.8

Citation: Kigozi M, Koech RK, Orisekeh K, Kali R, LM Kamoga O, et al. (2023) Porous carbon derived from *Zea mays* cobs as excellent electrodes for supercapacitor applications. Open J Anal Bioanal Chem 7(1): 001-010. DOI: https://dx.doi.org/10.17352/ojabc.000028

Electrochemical characterization of materials

The performance of as-prepared electrode materials was first tested in the three-electrode system using 6 M KOH as the electrolyte. The CV curves for ANN6, ANN7, and ANN8 at a scan rate of 10 mV/s are shown in Figure 6a. Sample ANN7 exhibited a slight discharge hump near 0.8 V due to some redox pseudocapacitance of the functional groups. All the CV curves exhibited a quasi-rectangular-like shape throughout the scanning range showing the good performance of EDLC [34,39]. The GCD curves for all the materials, as shown in Figure 6b, indicated an isosceles triangular shape for the GCD profile carried at 0.25 A/g. This confirmed the dominant EDLC behavior for the electrode material. Using the discharge time at different current densities, the specific capacitance was determined using equation one for the three samples, as shown in Figure 6c. The highest specific capacitance of ANN6, ANN7, and ANN8 are 537.3 F/g at 0.5 A/g, 517.5 F/g at 0.5 A/g and 389.7 F/g at 0.25 A/g respectively. The other GCD plot for the samples exhibited the same V-shape at different current densities, as shown in Figure S2 (Supplementary information).

The samples had an excellent specific surface area that corresponded to performance. The possible interaction of electrolyte ions and suitable porous surfaces of the materials, as well as the heteroatomic function groups on the surface wettability, all impact performance. As shown in Figure 1, the materials' sheet-like structure exposes the active areas for comprehensive interface interaction between electrode surfaces and electrolyte ions. The findings are comparable to those published in the literature [12,40-42].

The Electrochemical (EC) properties of the synthesized materials, including specific capacitance, energy density, power density, and stability, were determined objectively. The materials were tested using a two-electrode configuration method. The CV was performed at various scanning rates ranging from 5 mV/s to 200 mV/s with a potential range ranging from 0 to 1.0 V, resulting in quasi-rectangular forms, as illustrated in Figure 7. Figure 8 shows the GCD of the materials at varied current densities ranging from 0.25 to 2.5 A/g and exhibiting V-shapes. As demonstrated in Figure 6, the CV and GCD curves tested in the two-electrode system exhibit no significant differences in shape compared to those evaluated in the three-electrode system (a & b). In Figure 7, the CV for the as-prepared electrode materials has comparable quasi-

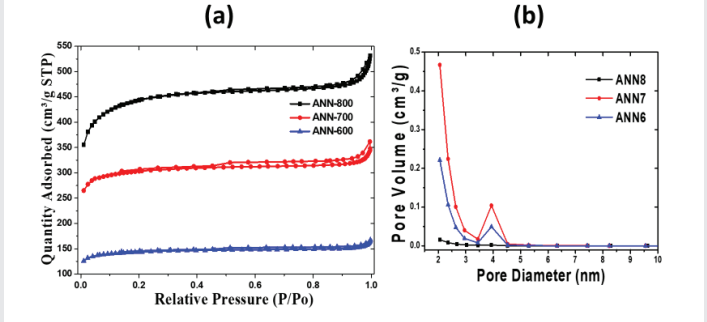

Figure 5: (a) N_2 adsorption-desorption isotherms and (b) Pore size distribution of the activated carbon samples from the BET analysis.

Table 4: The pore characteristics of ANN6, ANN7, and ANN8 activated carbon samples.

Sample	S_{BET} (m^2/g)	S_{mic} (m^2/g)	S_{mic}/S_{BET} (%)	S_{ext} (m^2/g)	V_{micro} (cm^3/g)	V_{meso} (cm^3/g)	V_{total} (cm^3/g)	V_{mic}/V_{tot} (%)
ANN6	461.36	385.66	83.6	75.71	0.1889	0.05749	0.2464	76.7
ANN7	972.65	689.28	70.87	460.76	0.3628	0.1682	0.5310	68.3
ANN8	1443.94	1000.89	69.30	383.05	0.5167	0.27485	0.7915	65.3

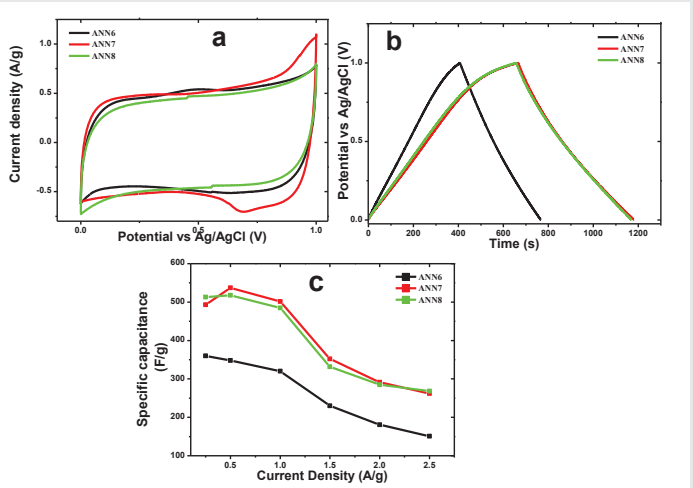

Figure 6: (a) C.V.s at a scan rate of 10 mV/s, (b) GCD carried at a current density of 0.25 A/g, (c) specific capacitance with different current densities of ANN6, ANN7 and ANN8 activated carbon samples.

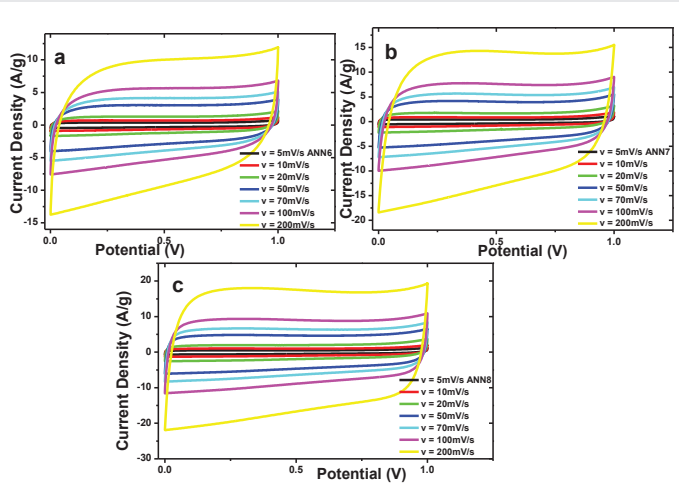

Figure 7: CV curves for (a) ANN6, (b) ANN7 and (c) ANN8 activated carbon samples at different scan rates.

rectangular forms. The ANN6 (Figure 7a) displayed a redox reaction at the lower and upper potentials. This phenomenon was also seen in the ANN7 sample (Figure 7b), although with fewer redox peaks. This could be owing to the reversible redox reaction between functional groups derived primarily from quinone or carbonyl (R) functional groups and the electrolyte, as shown in equation 5.

$$R-C_X-O+H^+ +e^- \leftrightarrow R-C_X-OH \quad (5)$$

The ANN8 sample had quasi-rectangular forms but did not undergo the Faradaic process. This could be due to the ANN8 sample's consistent porosity, as illustrated in Figure 1 (ANN8),

Citation: Kigozi M, Koech RK, Orisekeh K, Kali R, LM Kamoga O, et al. (2023) Porous carbon derived from *Zea mays* cobs as excellent electrodes for supercapacitor applications. Open J Anal Bioanal Chem 7(1): 001-010. DOI: https://dx.doi.org/10.17352/ojabc.000028

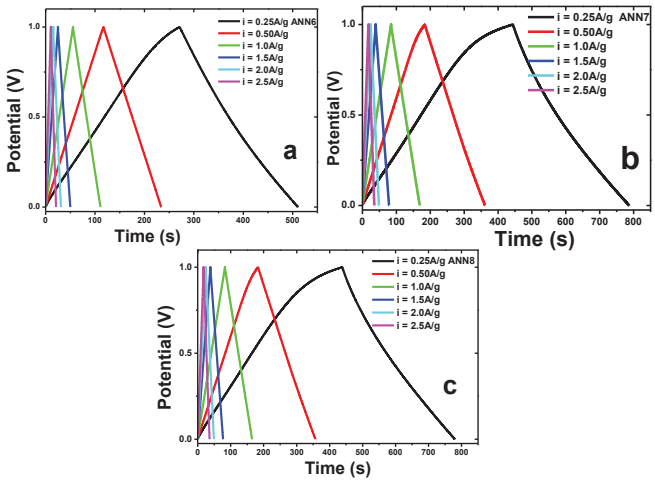

Figure 8: GCD curves for (a) ANN6, (b) ANN7 and (c) ANN8 activated carbon samples at different current densities.

which differs from others. All tested materials demonstrated identical shapes at even greater rates of 200 mV/s without altering the shapes, suggesting the materials' remarkable stability. This also means that the materials have a high charge-discharge capacity [33,43]. The exhibited symmetrical rectangular shapes indicated better performance than most reported results in the literature [10,34,39,40]. After stability, the CVs exhibited less or no exponential for the faradaic process, indicating no pseudocapacitance after holding the electrode materials at the high potential for a total of 130 h as shown in Figure S3(a-f) (supplementary information) at a scan rate of 5 mV/s.

The GCD was performed at various specific currents to investigate the specific capacitance performance of the materials using a two-electrode system setup. As illustrated in Figure 8, the GCD curves were essentially symmetrical triangular V-shapes, demonstrating a characteristic trait for good EDLC properties. This shows that the materials have no Faradaic process, which usually results in poor stability performance. The GCD characteristics match the CV performance in Figure 7 exceptionally well. The charge-discharge behavior was consistent for the three-electrode system (Figure 6b) and the two-electrode arrangement. For ANN6, ANN7, and ANN8 materials, the electrochemical (EC) assessment for specific capacitance was computed using equation (2), taking the mass loading of the two electrodes as total mass [2,3]. The computed specific capacitance values of the devices varied with the applied current densities, as shown in Figure S4a (supplementary information). At 0.5 A/g, the most significant specific capacitance of the ANN7 sample material was 358.7 F/g. For all sample materials, the specific capacitance of the built devices declined with increasing current densities (Figure S4a supplementary information). This mainly results from limited electrolyte ion transport and interaction at the electrode interface at higher current densities [44]. The ANN8 exhibited a maximum specific capacitance of 347.8 F/g at 0.5 A/g current density. Also, ANN6 presented its highest specific capacitance of 241.3 F/g 0.25 A/g current density.

The energy density and the power density of the assembled devices were calculated according to equations (3) and (4), respectively, as presented in the Ragone plot shown in Figure S4b (supplementary information) for all the sample materials. The device assembled from ANN7 presented the highest energy density of 12.45 Wh/kg for a current density of 0.5 A/g with a corresponding power density of 250 W/kg. This result is comparable and even higher than the symmetric assembled EDLC supercapacitors (SCs) reported in the literature [3,4,7,8]. The ANN6 sample material exhibited an energy density of 8.38 Wh/kg for a power density of 125 W/kg at a current density of 0.25A/g. The ANN8 sample material also presented an energy density of 12.08 Wh/kg with a corresponding power density of 250 W/kg at 0.5 A/g current density [45]. The energy density is approximately the same as that of the ANN7 sample, which can further be tested for commercial application of different supercapacitors.

To determine the resistive behavior of the electrode materials for supercapacitor application, electrochemical impedance spectroscopy (EIS) was performed on all sample materials. The EIS was measured at a potential of 10 mV in the frequency range of 10 kHz to 10 MHz. Figure 9 shows the Nyquist plot of the sample materials zoomed at high frequency in the insert, and Figure S5 (Supplemental information) exposes the semicircle. The small semicircles on the real axis indicate low charge transfer resistance (RCT) at the sample interface, implying good electrochemical performance [2]. The highest resistance was demonstrated by the ANN7 sample material, which had an RCT of 2.5Ω, while the ANN6 and ANN8 samples had RCTs of 1.1 and 1.3Ω, respectively. The vertical behavior with the imaginary axis at low frequency indicates low ion diffusion into the pores of the electrode materials shown in Figure 9. This indicates that the materials have excellent cycling stability and capacitive performance. The sample materials were also tested at 20 mV to see how the plots behaved at higher potentials, as shown in Figure S5. This suggested that the behavior was comparable at high frequencies with a modest variance at a lower frequencies. This shows some ion diffusion into the sample pores at higher potentials.

The stability test of the as-prepared devices was evaluated using the voltage holding / floating method. The three sample materials exhibited almost no degradation for the devices' electrochemical performance, showing uniform behavior as

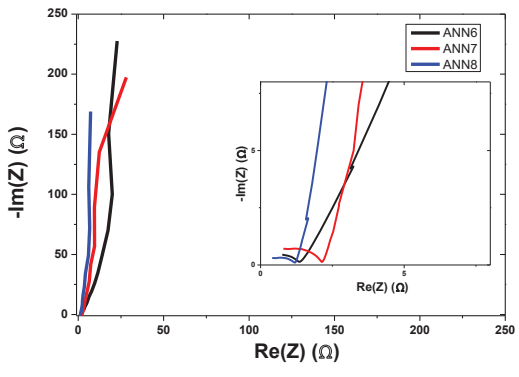

Figure 9: Figure EIS for ANN6, ANN7 and ANN8 activated carbon scanned at 10 mV; Insert is the zoomed high frequency.

Citation: Kigozi M, Koech RK, Orisekeh K, Kali R, LM Kamoga O, et al. (2023) Porous carbon derived from *Zea mays* cobs as excellent electrodes for supercapacitor applications. Open J Anal Bioanal Chem 7(1): 001-010. DOI: https://dx.doi.org/10.17352/ojabc.000028

shown in Figure S6, S7 (Supplementary information). The stability was achieved by holding the assembled device at a maximum potential of 1.0 V for 10 h after every three charge-discharge cycles repeated for 130 h at 0.5 A/g. The capacitance of the assembled devices remained almost constant throughout 130 h with no prominent decrease with increased time and cycling. This indicates that there was uniform wettability throughout the electrode/electrolyte ion interaction, and there were no trapped ions in the pores of the large porosity of the as-prepared electrode material [1]. The SCs showed excellent stability with 99% retention of the initial specific capacitance value even after 130 h holding. This excellent stability of the assembled devices is attributed to the microporous nature of the prepared sample material that keeps the uniform wettability and easy access to electrolytic ion movement. The self-discharge test was carried out on the assembled devices after voltage holding to determine the life span. In the test, the device was fully charged to a maximum potential of 1.0 V at 0.5 A/g, then held for 5 min before undergoing a self-discharge in an open circuit. Figure S8 (Supplementary information) exhibited an immediate drop for ANN6 sample material and lost 70% of the potential within 20 min. ANN7 and ANN8 showed a linear drop of potential losing 70% approximately after 4hrs and 3hrs, respectively. The potential drop may be due to the decomposition of water used in the electrolyte at higher potential since ionic strength depends on the electrolyte, and the water splitting requires a minimum potential difference of approximately 1.23 V.

Conclusion

The porous carbon (ANN) generated from *Zea mays* (maize) cobs was successfully tuned at different temperatures using KOH as the activation agent in a 1:4 ratio under a nitrogen atmosphere. At rising temperatures, the activated porous carbon demonstrated a tremendous increase in specific surface area and porosity. The sample materials exhibited optimal surface functional groups of oxygen base, resulting in outstanding electrochemical performance and stability for supercapacitor applications. For more than 130 hours of repeated maximum voltage holding, the samples demonstrated 99% stability. The symmetrically built ANN7 device with 5 M KOH electrolyte in a two-electrode configuration system demonstrated a maximum specific capacitance of 358.7 F/g, an energy density of 12.45 Wh/kg at 0.5 A/g, and capacitance retention of 99% after 130 hours of repeated voltage floating. This study discovered that increasing the temperature of activation of activated carbon from biomass improves the electrochemical performance of supercapacitors. Furthermore, activated carbon from *Zea mays* cobs combined with an appropriate activation agent can provide better-performing electrode materials for various supercapacitor applications at 700 °C as the optimum temperature.

Funding

This work was sponsored by the MAPRONANO ACE Makerere University project (P151847 / IDA 5797-UG) and supported by both the India- DST World Bank Cooperation on Strengthening of African Centres of Excellence (Grant No: DST/INT/AFRICA/ACEs/2016) and the African Development Bank and Pan African Materials Institute at the African University of Science and Technology (Grant No: PAMI/2015/5415-NG).

Authors' contributions

N Y D, A P O, P K J, JBK, and GNK conceptuses, designed and supervised the experiments and ran the work's administrative part. MK, R K, BP, AB, R K K, K O and OL M K performed synthesis and characterization studies and made the first draft. All the authors reviewed and agreed on this version of the manuscript.

Acknowledgment

This research work was conducted under the INDO-African knowledge transfer program under the World Bank Development program. The authors thank ARCI under DST India for supporting this study through the research fellowship scheme. M.K. acknowledges Dr. P.K Jain from ARCI and Annet Nanyitti for support. N.Y.D. acknowledges the UK Engineering and Physical Sciences Research Council (EPSRC) for funding (Grant No. EP/S001395/1).

(**Supplementary information is available**)

References

1. Tarimo DJ, Oyedotun KO, Mirghni AA, Sylla NF, Manyala N. High energy and excellent stability asymmetric supercapacitor derived from sulphur-reduced graphene oxide/manganese dioxide composite and activated carbon from peanut shell. Electrochim Acta. 353(136498):1–12, 2020, doi: 10.1016/j.electacta.2020.136498.

2. Kigozi M. Synthesis and characterization of graphene oxide from locally mined graphite flakes and its supercapacitor applications. Results Mater. 2020; 7: 100113. doi: 10.1016/J.RINMA.2020.100113.

3. Rajesh M. Pinecone biomass-derived activated carbon : the potential electrode material for the development of symmetric and asymmetric supercapacitors. Energy Res. 2020; 1-15. doi: 10.1002/er.5548.

4. Hsiao C, Lee C, Tai N. Biomass-derived three-dimensional carbon framework for a flexible fibrous supercapacitor and its application as a wearable smart textile. RSC Adv. 2020 Feb 17;10(12):6960-6972. doi: 10.1039/c9ra07441d. PMID: 35493907; PMCID: PMC9049747.

5. Kigozi M, Kali R, Bello A, Padya B, Kalu-Uka GM, Wasswa J, Jain PK, Onwualu PA, Dzade NY. Modified Activation Process for Supercapacitor Electrode Materials from African Maize Cob. Materials (Basel). 2020 Nov 27;13(23):5412. doi: 10.3390/ma13235412. PMID: 33261206; PMCID: PMC7731031.

6. Malothu RU, Nanaji K, Narasinga TR, Suresh AD. Corn husk derived activated carbon with enhanced electrochemical performance for high-voltage supercapacitors. J Power Sources. 2020; 471: 228387. doi: 10.1016/j.jpowsour.2020.228387.

7. Inal IIG, Aktas Z. Applied Surface Science Enhancing the performance of activated carbon based scalable supercapacitors by heat treatment. Appl Surf Sci. 2020; 514:145895. doi: 10.1016/j.apsusc.2020.145895.

8. Wang J, Li Q, Peng C, Shu N, Niu L, Zhu Y. To increase electrochemical performance of electrode material by attaching activated carbon particles on reduced graphene oxide sheets for supercapacitor. J Power Sources. 2019; 450: 227611. doi: 10.1016/j.jpowsour.2019.227611.

9. Xie X. Dielectric parameters of activated carbon derived from rosewood and corncob. J Mater Scie Mater Electron. 2020; 8. doi: 10.1007/s10854-020-04358-8.

Citation: Kigozi M, Koech RK, Orisekeh K, Kali R, LM Kamoga O, et al. (2023) Porous carbon derived from *Zea mays* cobs as excellent electrodes for supercapacitor applications. Open J Anal Bioanal Chem 7(1): 001-010. DOI: https://dx.doi.org/10.17352/ojabc.000028

10. Nguyen TN, Le PA, Phung VBT. Facile green synthesis of carbon quantum dots and biomass-derived activated carbon from banana peels : synthesis and investigation. Biomass Convers. Biorenery. 2020; doi: 10.1007/s13399-020-00839-2.

11. Lin Y, Chen Z, Yu C, Zhong W. Electrochimica Acta Facile synthesis of high nitrogen-doped content , mesopore-dominated biomass-derived hierarchical porous graphitic carbon for high performance supercapacitors. Electrochem Soc. 2020; 148: A149. 334:135615.

12. Liu M, Li W, Ruan S, Fei Y. N - doped Hierarchical Mesoporous Carbon from Mesophase Pitch and Polypyrrole for Supercapacitors. Energy and Fuels. 2020; 34: 5044–5052. doi: 10.1021/acs.energyfuels.0c00176.

13. Inagaki M, Konno H, Tanaike O. Carbon materials for electrochemical capacitors. J Power Sources. 2010; 195: 7880–7903. doi: 10.1016/j.jpowsour.2010.06.036.

14. Centeno TA, Sevilla M, Fuertes AB, Stoeckli F. On the electrical double-layer capacitance of mesoporous templated carbons. Carbon NY; 2005; 43:3012–3015.

15. Zhi M, Xiang C, Li J, Li M, Wu N. Nanostructured carbon-metal oxide composite electrodes for supercapacitors: a review. Nanoscale. 2013 Jan 7;5(1):72-88. doi: 10.1039/c2nr32040a. Epub 2012 Nov 15. PMID: 23151936.

16. Zhi M, Yang F, Meng F, Li M, Manivannan A, Wu N. Effects of Pore Structure on Performance of An Activated-Carbon Supercapacitor Electrode Recycled from Scrap Waste Tire. ACS Sustain Chem Eng. 2014.

17. Lu H, Zhao X. Biomass-derived carbon electrode materials for supercapacitors. Sustain Energy Fuels. 1:265-1281. 2017, doi: 10.1039/C7SE00099E.

18. Raj CJ. High electrochemical capacitor performance of oxygen and nitrogen enriched activated carbon derived from the pyrolysis and activation of squid gladius chitin. J Power Sources. 2018; 386: 66–76. doi: 10.1016/j.jpowsour.2018.03.038.

19. Nankya R, Lee J, Opar DO, Jung H. Electrochemical behavior of boron-doped mesoporous graphene depending on its boron configuration. Appl Surf Sci. 2019; 489: 552–559. doi: 10.1016/j.apsusc.2019.06.015.

20. Lim WC, Srinivasakannan C, Balasubramanian N. Activation of palm shells by phosphoric acid impregnation for high yielding activated carbon. J Anal Appl Pyrolysis. 2010; 88: 181–186. doi: 10.1016/j.jap.2010.04.004.

21. Le Van K, Thuy T, Thi L. Activated carbon derived from rice husk by NaOH activation and its application in supercapacitor. Prog Nat Sci Mater Int. 2014; 24:191–198. doi: 10.1016/j.pnsc.2014.05.012.

22. Lijuan H, Peng Y, Feng W, Peng S, Jin Jun L, Zizheng L. Tubular activated carbons made from cotton stalk for dynamic adsorption of airborne toluene. J Taiwan Inst Chem Eng. 2017; 80:399-405. doi: 10.1016/j.jtice.2017.07.029.

23. Shafeeyan MS, Wan MWA, Houshmand A, Shamiri A. A review on surface modification of activated carbon for carbon dioxide adsorption. J Anal Appl Pyrolysis. 2010; 89:143-151. doi: 10.1016/j.jaap.2010.07.006.

24. Elmouwahidi A, Esther BG, Agustin FPC, Francisco JMH, Francisco CM. Activated carbons from KOH and H3PO4-activation of olive residues and its application as supercapacitor electrodes. Electrochim Acta. 2017; 229:219–228. doi: 10.1016/j.electacta.2017.01.152.

25. Barzegar F. Cycling and floating performance of symmetric supercapacitor derived from coconut shell biomass. AIP Adv. 6(115306): 2016. doi: 10.1063/1.4967348.

26. Moyo B, Momodu D, Fasakin O, Dangbegnon J, Manyala N. Materials Electrochemical analysis of nanoporous carbons derived from activation of polypyrrole for stable supercapacitors. Energy Mater. 53:5229–5241, 2018, doi: 10.1007/s10853-017-1911-y.

27. Bello A. Floating of PPY Derived Carbon Based Symmetric Supercapacitor in Alkaline Electrolyte. ECS Soc Electrochem. 2017; 75: 1-12. doi: 10.1149/07524.0001ecst.

28. Wei H. Advanced porous hierarchical activated carbon derived from agricultural wastes toward high performance supercapacitors. Alloy Compd. 2019. doi: 10.1016/j.jallcom.2019.153111.

29. Wang CH, Wen WC, Hsu HC, Yao BY. High-capacitance KOH-activated nitrogen-containing porous carbon material from waste coffee grounds in supercapacitor. Adv Powder Technol. 2016; 27:1387–1395. doi: 10.1016/j.apt.2016.04.033.

30. Yang J, Xiang F, Guo H, Wang L, Niu X. Honeycomb-like porous carbon with N and S dual-doping as metal- free catalyst for the oxygen reduction reaction. Carbon NY. 2020; 156:514-522. doi: 10.1016/j.carbon.2019.09.087.

31. Sudhan N, Subramani K, Karnan M, Ilayaraja N, Sathish M. Biomass-derived activated porous carbon from rice straw for a high-energy symmetric supercapacitor in aqueous and nonaqueous electrolytes. Energy and Fuels. 2017; 31:977–985. doi: 10.1021/acs.energyfuels.6b01829.

32. Qiu X, Wang L, Zhu H, Guan Y, Zhang Q. Lightweight and efficient microwave absorbing materials based on walnut shell-derived nano-porous carbon. Nanoscale. 2017 Jun 8;9(22):7408-7418. doi: 10.1039/c7nr02628e. PMID: 28540377.

33. Zequine C, Ranaweera CK, Wang Z, Singh S, Tripathi P, Srivastava ON, Gupta BK, Ramasamy K, Kahol PK, Dvornic PR, Gupta RK. High Per formance and Flexible Supercapacitors based on Carbonized Bamboo Fibers for Wide Temperature Applications. Sci Rep. 2016 Aug 22;6:31704. doi: 10.1038/srep31704. PMID: 27546225; PMCID: PMC4992840.

34. Ji L. N, S co-doped biomass derived carbon with sheet-like microstructures for supercapacitors. Electrochem Acta. 2019; 19. doi: 10.1016/j.electacta.2019.135348.

35. Zhao H, Lu X, Wang Y, Sun B, Wu X, Lu H. Effects of additives on sucrose-derived activated carbon microspheres synthesized by hydrothermal carbonization. J Mater Sci. 2017; 52:10787–10799. doi: 10.1007/s10853-017-1258-4.

36. Chen W, Hu C, Yang Y, Cui J, Liu Y. Rapid Synthesis of Carbon Dots by Hydrothermal Treatment of Lignin. Materials (Basel). 2016 Mar 9;9(3):184. doi: 10.3390/ma9030184. PMID: 28773309; PMCID: PMC5456677.

37. Liu B, Liu Y, Chen H, Yang M, Li H. Oxygen and nitrogen co-doped porous carbon nanosheets derived from Perilla frutescens for high volumetric performance supercapacitors. J Power Sources. 2017; 341: 309-317. doi: 10.1016/j.jpowsour.2016.12.022.

38. Peng L. Super-hierarchical porous carbons derived from mixed biomass wastes by a stepwise removal strategy for high-performance supercapacitors. J Power Sources. 2018;377:151–160. doi: 10.1016/j.jpowsour.2017.12.012.

39. Chen Y. Synthesis of porous NiCoS nanosheets with Al leaching on ordered mesoporous carbon for high-performance supercapacitors. Chem Eng Jounal. 2019. doi: 10.1016/j.cej.2019.123367.

40. Juan D, Zhang Y, Wu H, Hou S, Chen A. N-doped hollow mesoporous carbon spheres by improved dissolution-capture for supercapacitors. Carbon NY. 2020; 156: 523–528. doi: 10.1016/j.carbon.2019.09.091.

41. Li R, Zhou Y, Li W, Zhu J, Huang W. Structure Engineering in Biomass-Derived Carbon Materials for Electrochemical Energy Storage. Research (Wash D C). 2020 Apr 29;2020:8685436. doi: 10.34133/2020/8685436. PMID: 32426728; PMCID: PMC7206893.

42. Lokhande PE, Chavan US, Pandey A. Materials and Fabrication Methods for Electrochemical Supercapacitors : Overview. 2019.

43. Liu J, Deng Y, Li X, Wang L. Promising Nitrogen-Rich Porous Carbons Derived from One-Step Calcium Chloride Activation of Biomass-Based Waste for High Performance Supercapacitors. ACS Sustain Chem Eng. 2016; 177-187. doi: 10.1021/acssuschemeng.5b00926.

Citation: Kigozi M, Koech RK, Orisekeh K, Kali R, LM Kamoga O, et al. (2023) Porous carbon derived from *Zea mays* cobs as excellent electrodes for supercapacitor applications. Open J Anal Bioanal Chem 7(1): 001-010. DOI: https://dx.doi.org/10.17352/ojabc.000028

44. Raj CJ. Two-Dimensional Planar Supercapacitor Based on Zinc Oxide/Manganese Oxide Core/Shell Nano-architecture. Electrochim Acta. 2017; 247: 949-957. doi: 10.1016/j.electacta.2017.07.009.

45. Kigozi M, Ezealigo BN, Kasozi GN, Tebandeke E, Kirabira JB. The Science of High-Energy Graphene Oxide–Based Materials for Hybrid Energy Storage Applications. In Graphene Oxide in Enhancing Energy Storage Devices, Boca Raton: CRC Press, 2022; 151–192. doi: 10.1201/9781003215196-11.

Citation: Kigozi M, Koech RK, Orisekeh K, Kali R, LM Kamoga O, et al. (2023) Porous carbon derived from *Zea mays* cobs as excellent electrodes for supercapacitor applications. Open J Anal Bioanal Chem 7(1): 001-010. DOI: https://dx.doi.org/10.17352/ojabc.000028